Metamaterial adhesives for programmable adhesion through reverse crack propagation

Dohgyu Hwang^{1,2}, Chanhong Lee², Xingwei Yang³, Jose M. Pérez-González⁴, Jason Finnegan⁵, Bernard Lee⁵, Eric J. Markvicka⁵, Rong Long³, and Michael D. Bartlett^{1,2*}

¹Macromolecules Innovation Institute, Virginia Tech, Blacksburg, VA 24061, USA
²Department of Mechanical Engineering, Soft Materials and Structures Lab, Virginia Tech, Blacksburg, VA 24061, USA

³Department of Mechanical Engineering, University of Colorado, Boulder, CO 80309, USA
⁴Department of Materials Science & Engineering, Iowa State University, Ames, IA 50011, USA
⁵Department of Mechanical & Materials Engineering, Smart Materials and Robotics Lab, University of Nebraska–Lincoln, Lincoln, NE 68588, USA
*email: mbartlett@vt.edu

Cite this article: Hwang, D., *et al.* Metamaterial adhesives for programmable adhesion through reverse crack propagation. *Nat. Mater.* **22**, 1030–1038 (2023). https://doi.org/10.1038/s41563-023-01577-2

This version of the article has been accepted for publication, after peer review (when applicable) and is subject to Springer Nature's AM terms of use, but is not the Version of Record and does not reflect post-acceptance improvements, or any corrections. The Version of Record is available online at: https://doi.org/10.1038/s41563-023-01577-2

Abstract

Adhesives are typically either strong and permanent or reversible with limited strength. However, current strategies to create strong yet reversible adhesives needed for wearable devices, robotics, and material disassembly lack independent control of strength and release, require complex fabrication, or only work in specific conditions. Here we report metamaterial adhesives that simultaneously achieve strong and releasable adhesion with spatially selectable adhesion strength through programmed cut architectures. Non-linear cuts uniquely suppress crack propagation by forcing cracks to propagate backwards for 60x enhancement in adhesion, while allowing crack growth in the opposite direction for easy release and reusability. This mechanism functions in numerous adhesives on diverse substrates in wet and dry conditions and enables highly tunable adhesion with independently programmable adhesion strength in two directions simultaneously at any location. We create these multifunctional materials in a maskless, digital fabrication framework to rapidly customize adhesive characteristics with deterministic control for next-generation adhesives.

Main

Adhesive strength is dictated by how cracks move across a bonded interface.¹⁻⁴ By suppressing crack propagation, strong adhesives are created but are difficult to remove, while reusable adhesives promote separation which limits strength. This makes adhesives commonly either permanent and strong or reversible with limited strength. However, many applications are increasingly in need of adhesives that overcome this tradeoff in properties and require strong adhesion with easy removal and extended reuse. This seemingly paradoxical combination of properties is important in applications such as robotics for locomotion and grasping, wearable electronics for strong attachment yet easy removal of devices to monitor health and deliver drugs, and manufacturing for assembly and then disassembly to reduce waste, re-purpose materials, and aid in recycling.⁵⁻¹⁰

Material approaches to control adhesion typically focus on tuning interfacial chemistry or dissipating mechanical energy.^{11–14} These material-based mechanisms can result in very strong adhesives, but often do not have mechanisms for release, reusability, or directionality (i.e. high strength in one direction relative to another), as dissipation near the crack tip is similar in all directions. Geometry and stiffness also control adhesion. This is achieved through nano-to-micron scale bio-inspired surface features,^{15–21} passively varying stiffness through material patterning or actively varying stiffness with switchable adhesives,^{22–29} or adding incisions, cuts, or discontinuities into adhesives.^{30–34} These features blunt or trap cracks, which then reinitiate and propagate again in the original, forward direction.³¹ This increases adhesion force but does not necessarily facilitate directionality or release. Directional strength can be achieved,³⁵ but it is difficult to raise adhesion strength and directionality, as geometric mechanisms typically result in adhesion strengths below material-based mechanisms. Strategies that leverage both material and geometric mechanisms through accessible fabrication approaches can open synergistic opportunities to systematically suppress crack propagation for strong adhesion yet facilitate crack propagation for release and reusability.

Here we introduce a metamaterial adhesive that enables strong and reversible adhesion with directional, spatially selective adhesive strength through programmed non-linear cut architectures in adhesive films (Fig. 1a). The non-linear cuts consist of open polygonal shapes to control how adhesive cracks propagate by trapping cracks and then forcing them to reverse direction for high adhesion (Fig. 1b,c), and allowing them to propagate forward normally for low adhesion (Fig. 1d,e). Through reverse crack propagation, we decouple high global peel angles into low local peel angles at the adhesive interface. This mechanism enhances adhesion strength up to 60x for strong adhesion relative to the same material without cuts, while also enabling easy release on the order of an unpatterned adhesive by peeling in the opposite direction. These characteristics allow for independent control of adhesion strength and release with reusability. Reverse crack propagation also tunes adhesion strength at any film location and uniquely enables the programming of adhesive strength in two directions simultaneously in a single region of a film. Metamaterial adhesives do not rely on specific chemistry or environmental conditions, microstructured surfaces, or active or patterned stiffness to tune adhesion, but utilize non-linear cuts for highly systematic control of adhesive crack propagation and direction across a film.

We call these metamaterial adhesives as the non-linear cut architectures decouple global applied loads into a deterministic local adhesive response, leveraging insight from mechanical metamaterials which decouple local and global mechanical properties. 36-38 This functionality is intrinsic to the geometry and allows us to enhance properties and enable unique adhesion behavior in a wide range of adhesives, on diverse surfaces, and in dry and wet environments. This applicability to diverse materials allows metamaterial adhesives to leverage both material and geometric mechanisms to span a spectrum of unique adhesives properties, from strong and extremely reversible to extremely strong with reversibility, including adhesives with strengths over 3000 N/m (J/m²) that are also reusable and directional. These multifunctional metamaterial adhesives achieve highly systematic control of adhesive crack movement which allows us to achieve an unconventional combination of strong adhesion and easy release, programming of adhesive strength in two directions simultaneously, and applicability in numerous adhesives, while introducing a digital fabrication framework to automate design and rapidly manufacture adhesives in minutes with deterministic control of adhesive characteristics at any location across a film.

Characteristics of metamaterial adhesives

Our base metamaterial adhesive consists of a polydimethylsiloxane (PDMS) adhesive supported on an inextensible polyethylene terephthalate (PET) backing. Cut architectures are created in a digital design environment and are then rapidly patterned in the adhesive through a laser cutter. We define the *maximum* adhesion force (F_{max}) as the condition at which high adhesion is generated and the *minimum* adhesion force (F_{min}) as the condition at which low adhesion or easy release is attained. As adhesive force capacity for an adhesive material is higher at small peel angles,^{1,39} the selective decoupling of the global and local peel angles provides a mechanism to have a high adhesion in one direction (F_{max}) and easy release in the opposite direction (F_{min}).

Metamaterial adhesives are unique compared to a range of common reversible adhesives and strong adhesives, achieving Post-it[®] Note like easy release and reusability at F_{min} , with adhesive strength comparable to Duct tape at F_{max} (Fig. 1f). This dramatic difference in F_{max} and F_{min} can be observed by hanging a weight on the metamaterial adhesive, where the high strength holds the weight in the maximum force peel direction, yet the metamaterial adhesive releases rapidly in the minimum force peel direction (Fig. 1g and Supplementary Video 1). Adhesion enhancement with easy release is achieved for a variety of non-linear cut patterns including: triangular, rectangular, and hybrid cuts (peel curves in Supplementary Fig. 1). The rectangular and hybrid cuts display a \sim 60x increase, and triangular cuts a $\sim 40x$ increase over the unpatterned adhesive, quantified as the enhancement ratio $(F_{max}/F_{unpatterned})$ (Fig. 1h). This adhesion enhancement continues to function over 100 cycles (Supplementary Fig. 2). We quantify the adhesion directionality as F_{max}/F_{min} (Fig. 1i). The hybrid design shows the highest enhancement ratio $\sim 60x$ while showing exceptional easy release with an adhesion directionality ~ 25 (details of adhesion metrics are in Supplementary Note 1 and Supplementary Fig. 3 and mechanistic schematics in Supplementary Fig. 4 and 5). F_{min} can be tuned by modification of the cut structure into hybrid patterns, detuning of the adhesive layer through laser rastering, and adhesive material selection, which enables F_{min} to be equal to or lower than the unpatterned region of the film while maintaining high F_{max} (See Supplementary Fig. 6 and Fig. 7).

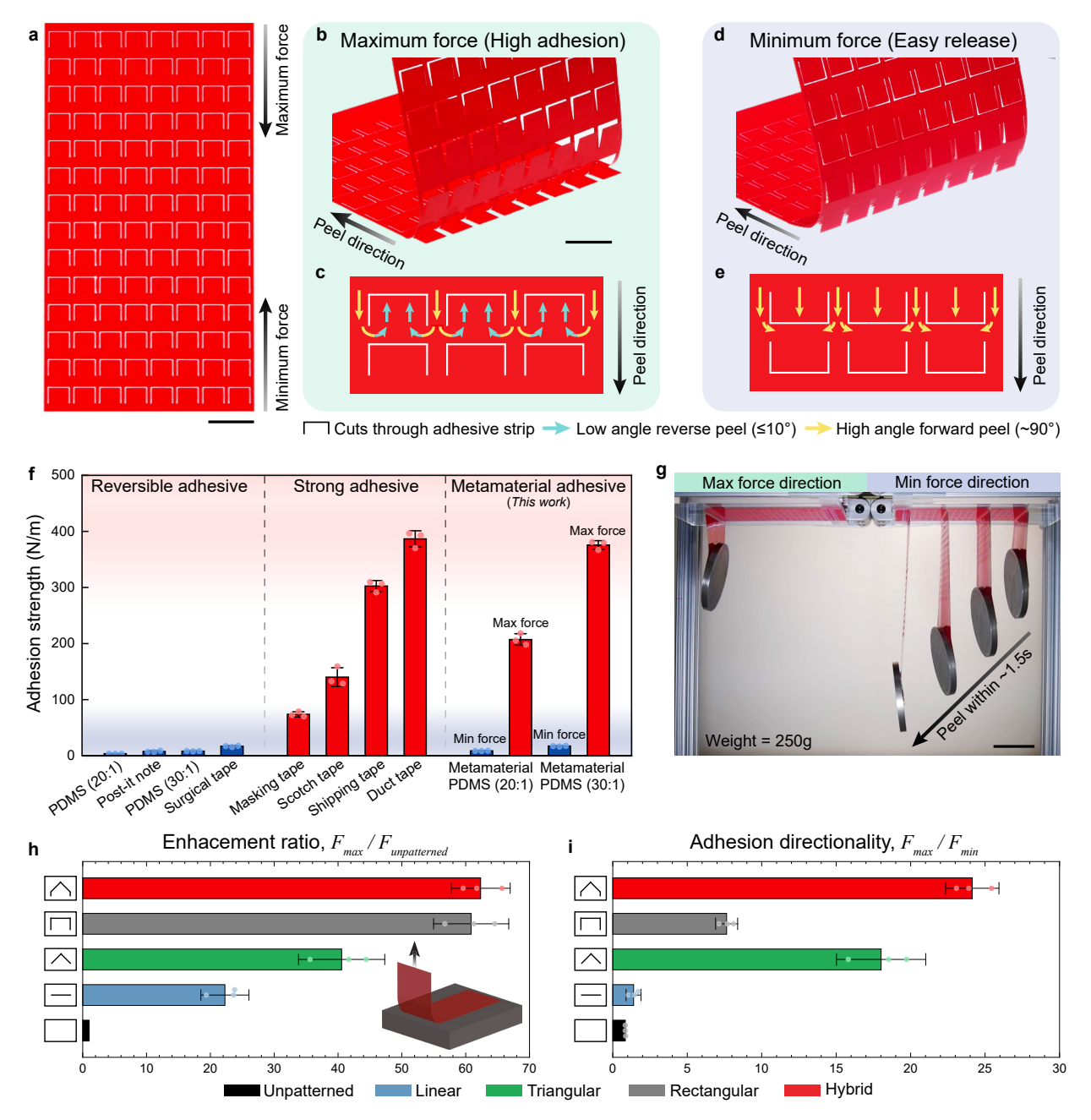


Fig. 1. High strength, easy release metamaterial adhesives. a, The metamaterial adhesive consists of cut patterns in an adhesive film. Scale bar = 15 mm. b, c, High adhesion is achieved in the maximum force direction when cracks propagate at low angles and reverse direction to propagate backwards to separate. Scale bar = 15 mm. **d**, **e**, Easy release is achieved in the minimum force direction as cracks continuously propagate forward to separate. f, Maximum force per total width, or max strength, of commercial adhesives and metamaterial adhesives. g, A metamaterial adhesive shows high adhesion (max force) and easy release (min force) in opposite peel directions. Scale bar = 50 mm. h, Adhesion enhancement ratios over an unpatterned adhesive for various cut shapes. i, Adhesion directionality for various cut shapes. Data are presented as the mean values \pm SD (n = 3 measurements from distinct samples for reversible and strong adhesive categories in \mathbf{f} and from the same sample measured repeatedly for each metamaterial adhesive in f, h, and i)

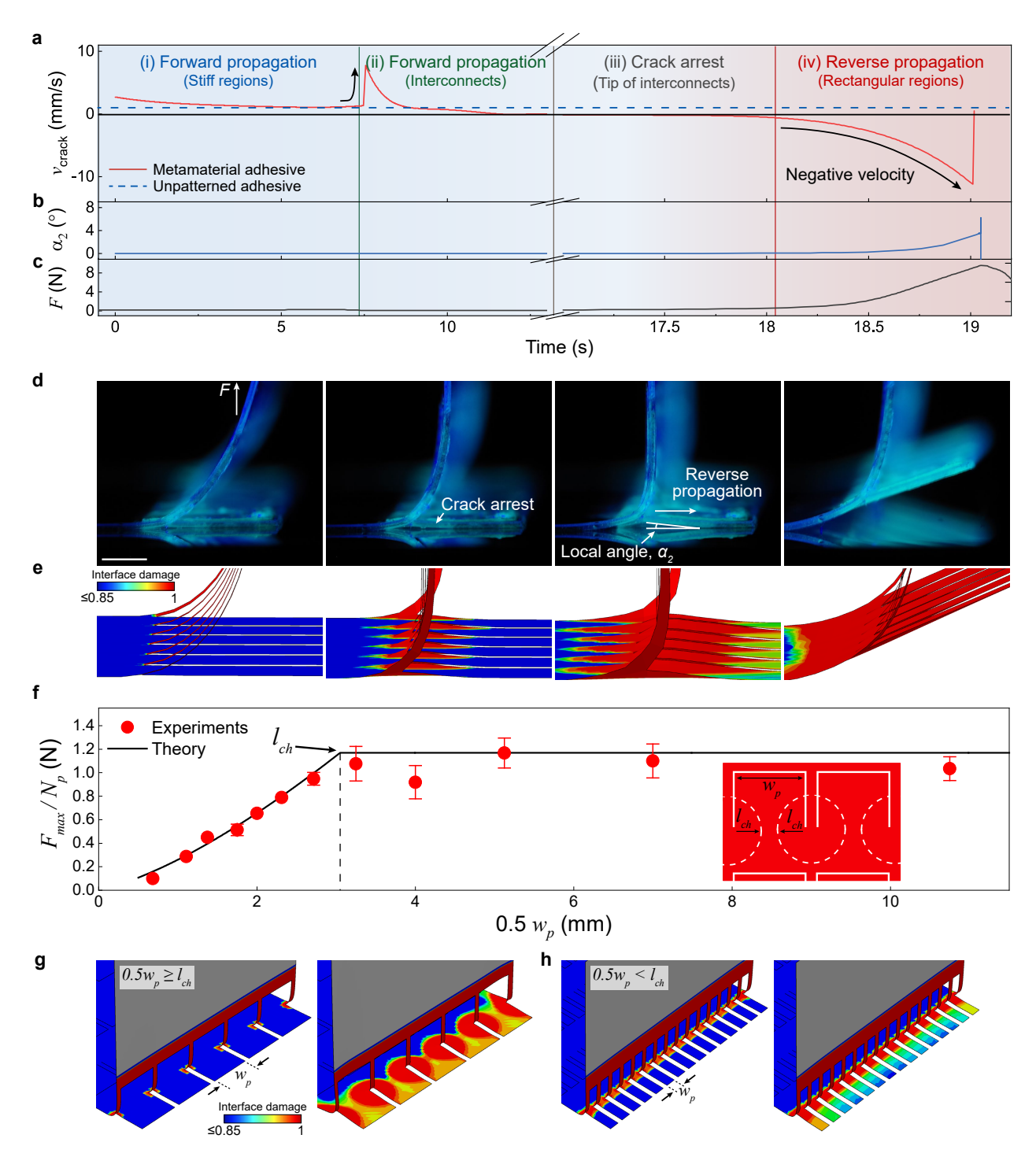


Fig. 2. Enhancing adhesion through reverse crack propagation. a, Crack velocity versus time for a metamaterial adhesive and unpatterned adhesive. **b**, Local peel angle near the crack tip from FEA. **c**, Measured force versus time of the metamaterial adhesive, **d**, Side profile images of a peeling adhesive (scale bar = 2 mm) and **e**, corresponding FEA results. **f**, Maximum force per cut pattern F_{max}/N_p versus half cut width $0.5w_p$. Solid line is the theoretical fit (Supplementary Note 3). **g-h**, FEA results showing crack arrest at interconnect tips (left) and crack morphology at $F = F_{max}$ (right) for **g**, $0.5w_p \ge l_{ch}$ and **h**, $0.5w_p < l_{ch}$. The color contours in **e**, **g-h** illustrate the interface damage that ranges from 0 (fully adhered) to 1 (completely delaminated). Data in **f** are presented as mean values \pm SD (n = 3 measurements from the same sample measured repeatedly).

Mechanistic description of reverse crack propagation

To understand the physical origin of the adhesion enhancement and directional release, we quantify the crack propagation behavior by plotting the crack front velocity versus time during a 90° peel experiment (Fig. 2a). While an unpatterned adhesive separates at a constant, positive velocity (i.e. forward), the metamaterial adhesive shows distinct crack dynamics (Supplementary Video 2). Initially, the crack propagates forward through the unpatterned region (zone i), accelerates as it passes through the interconnects (zone ii), and then is arrested at the base of the rectangular cut where the crack velocity drops to nearly zero and the applied force rises (zone iii). Further loading reverses the crack propagation direction, as indicated by the negative crack velocity, into the adhered rectangular regions at low peel angles (zone iv). In this stage, the local peel angle near the crack tip (α_2) and resultant adhesion force (F) start to increase, resulting in complete adhesive delamination and energy release (Fig. 2b and c). This reverse crack propagation at low angles is only present in the maximum force peeling direction and results in a dramatic rise in adhesive force, as observed in experiments (Fig. 2d and Supplementary Video 3) and captured in simulations using Finite Element Analysis (FEA) (Supplementary Note 2 and Supplementary Fig. 8). In the minimum force peel direction and in unpatterned adhesives the crack only propagates forward at low forces, as commonly observed in adhesive debonding. Linear cut patterns and closed-polygonal shaped incisions only show primarily forward or lateral crack propagation, 30,32 not systematic reverse crack propagation, which gives metamaterial adhesives superior enhancement, directionality and spatial control of adhesion.

The cut size is critical for achieving optimized adhesion enhancement. When the width w_p of rectangular cuts is varied with other dimensions fixed, the adhesion force per cut pattern, F_{max}/N_p , first increases with w_p and then saturates when $0.5w_p$ exceeds a critical value (Fig. 2f). The underlying mechanism is the transition between two distinct regimes of reverse crack propagation. When $0.5w_p$ exceeds a characteristic length l_{ch} , cracks originating at the tips of interconnects do not interfere with each other, leading to circular delaminated regions centered at each interconnect (Fig. 2g and Supplementary Fig. 9a). When $0.5w_p$ is smaller than l_{ch} , cracks from neighboring

interconnect tips merge before F_{max} is reached, resulting in an approximately uniform crack front during reverse crack propagation (Fig. 2h and Supplementary Fig. 9b). Theoretical analysis yields (Supplementary Note 3):

$$l_{ch} = \sqrt{\frac{2D}{G_c} \frac{w_{int}}{w} (N_p^* + 1)} \tag{1}$$

where D is the flexural rigidity of the adhesive film, w_{int} is the width of an interconnect, N_p^* is the optimal number of cut patterns that results in the highest F_{max} , w is the total width, and G_c is the critical energy release rate. While D, w_{int} , w and G_c are prescribed parameters, N_p^* can be either determined experimentally or solved algebraically (Supplementary Note 3). Theoretical analysis also shows that F_{max} is maximized when $0.5w_p = l_{ch}$ (Supplementary Note 3), making l_{ch} a key length for cut design.

Applicability in diverse materials, surfaces, and environments

To evaluate the versatility of the characteristic length l_{ch} , we applied rectangular cuts with different width w_p to various sets of adhesives, including PET/PDMS and commercial adhesives such as 3M Post-it® Note, 3M CoTranTM backing film/Dow Corning MG-7 9900 Soft Skin Adhesive, and 3M MicroporeTM. For each adhesive, the l_{ch} calculated using the theoretically solved N_p^* (Supplementary Note 3) agrees well with the experimentally determined N_p^* (Supplementary Table 1). In Fig. 3a the normalized maximum adhesive force for all of these different adhesives collapse onto a single master curve normalized by l_{ch} . This demonstrates that the metamaterial adhesive design approach is widely applicable to diverse materials and must be systematically designed around l_{ch} . Furthermore, other in-plane dimensions (spacing s, cut length l_p) must also be equal to or greater than l_{ch} . This avoids the premature interaction of adhesive cracks and allows for full adhesion enhancement (Supplementary Fig. 9 - Fig. 11), providing general guidance for metamaterial adhesive design.

The metamaterial adhesive strategy is applicable to diverse substrates and conditions. When we applied and measured the adhesive underwater, water is displaced and adhesion is enhanced

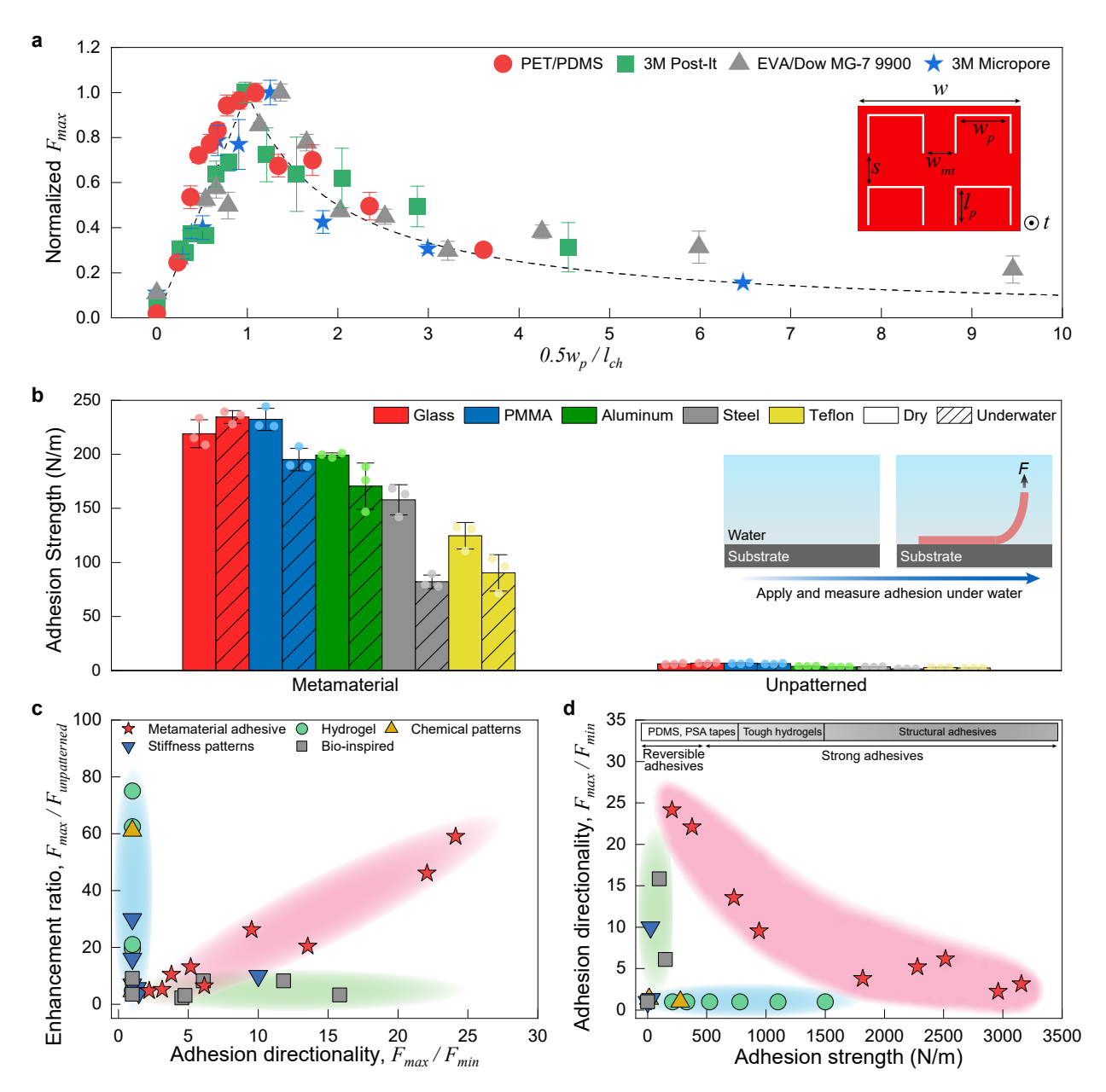


Fig. 3. Versatility and performance comparisons of metamaterial adhesives. **a**, Normalized maximum adhesion versus $0.5w_p/l_{ch}$ for different metamaterial adhesive materials, where the dashed line indicates a single master curve where experimental data points collapse. **b**, Maximum force per width of metamaterial adhesives versus unpatterned adhesives on diverse surfaces in dry and underwater environments. **c**, Comparison plots of Enhancement ratio versus Adhesion directionality and **d**, Adhesion directionality versus Adhesion strength show that metamaterial adhesives occupy unique regions of the adhesive property space. This comparison is for passive adhesives (i.e. no trigger release), no kinetic control (i.e. not comparing low to high testing rates), and on nominally smooth surfaces. See Supplementary Fig. 14 and Supplementary Table 2 for detailed identification of data points. Data in **a** and **b** are presented as mean values \pm SD (n = 3 measurements from the same sample measured repeatedly).

(at least 30x and up to 56x) relative to unpatterned adhesives on glass, plastic/PMMA, aluminum, steel, and Teflon (Fig. 3b and Supplementary Fig. 12 and Fig. 13). These results validate that metamaterial adhesives are applicable over a wide range of material types, substrates, and environments to enhance adhesion without specific chemistry or surface topology.

Performance of metamaterial adhesives

The adhesion performance of metamaterial adhesives are highlighted by comparing combinations of adhesion enhancement, directionality, and strength to previous literature results (Fig. 3c and d). Here we compare the metamaterial adhesives to hydrogels, ^{13,40–44} chemical patterns, ^{12,45,46} stiffness patterns, 3,23,30–32,47 and bio-inspired. 2,15,18,35,48–50 Fig. 3c shows that adhesives commonly show enhancement with little directionality (blue shaded region), or directionality with little enhancement (green shaded region), while metamaterial adhesives can be made with both high enhancement and directionality (red shaded region). Fig. 3d shows that typically directional adhesives show low strength (green shaded region) while high strength adhesives (blue shaded region) show little directionality. Metamaterial adhesives overcome these challenges and show unique adhesive properties, from strong and extremely directional (top-left quadrant) to extremely strong with directionality (bottom-right quadrant) while being reusable in all cases (red shaded region). This includes metamaterial adhesives with intrinsically strong acrylic adhesive layers such as 3M VHB (Very High Bond). This enhanced adhesion beyond the already strong unpatterned adhesive and increased strength (which is equivalent to adhesion toughness for 90° peeling) to over 3000 N/m (J/m²). Significantly, these very strong metamaterial adhesives were still directional and were reusable over multiple testing cycles (See Supplementary Fig. 2 for cyclic data), which is uncommon as strong adhesives typically rely on bonding mechanisms which are not directional and do not function beyond a single cycle. These types of properties demonstrate the versatility of metamaterial adhesives and open exciting performance characteristics for adhesive materials.

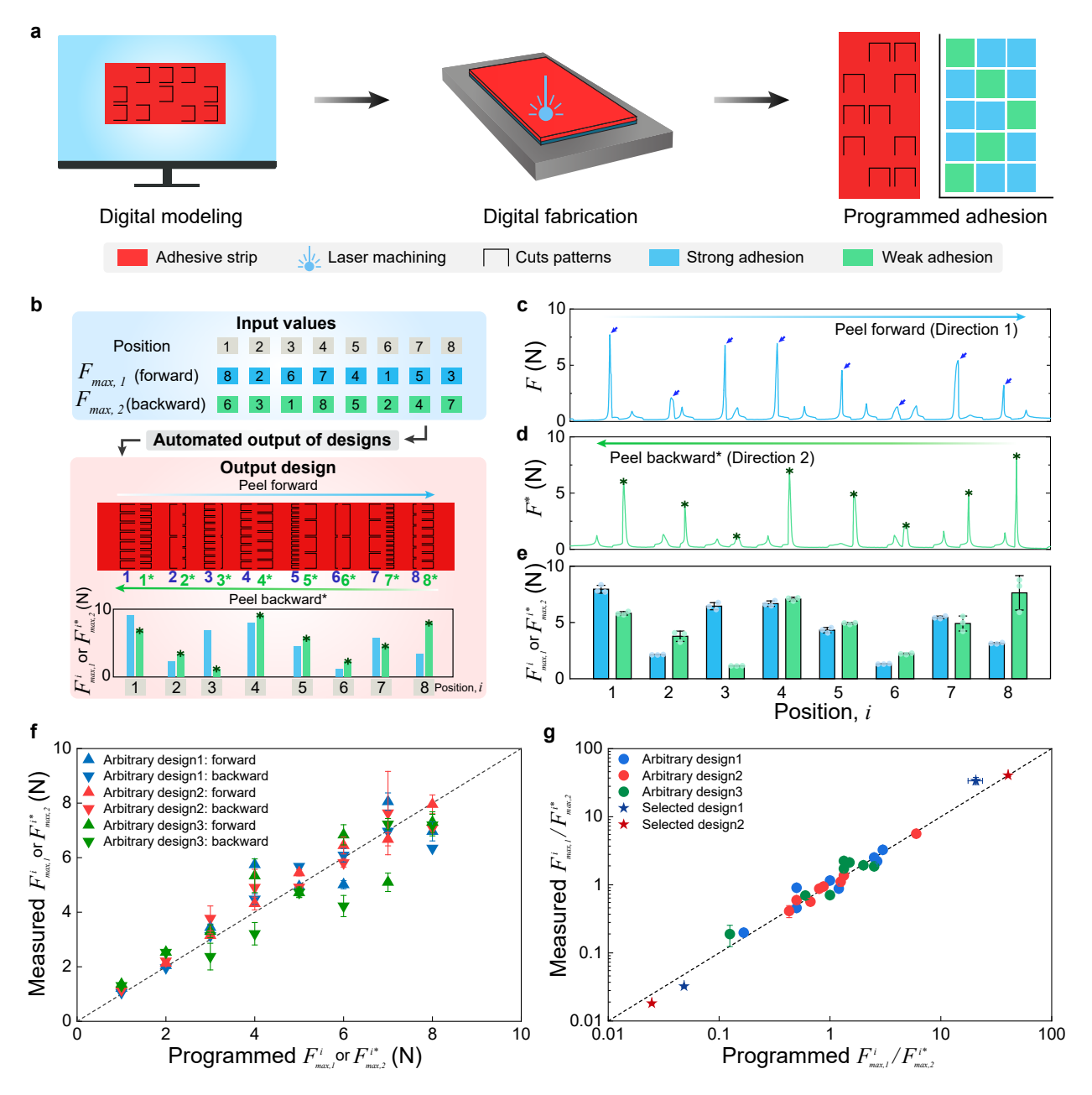


Fig. 4. Digitalized adhesive fabrication. a, Digital fabrication scheme for programmable metamaterial adhesives. **b**, Automated design generates a layout of programmed adhesion strength represented by the output design. **c**, Force versus position for the adhesive fabricated with the automated design in Fig. 4b in the forward direction and **d**, in the backward direction, with compiled data in **e** as a function of position. **f**, Measured and programmed maximum forces show excellent agreement. **g**, Decoupling of directionality, which creates maximum/maximum forces at each region in both forward/backward directions, shows good agreement with programmed and measured results for both arbitrary and selected designs. Data in **e**-**g** are presented as mean values \pm SD (n = 3 measurements from the same sample measured repeatedly).

Digital manufacturing and design of metamaterial adhesives

Metamaterial adhesives can enable spatial tunability of adhesion. We utilize digital fabrication with computer-aided design (CAD) and laser-based subtractive manufacturing to enable rapid, maskless fabrication of programmed adhesion profiles (Fig. 4a). As a demonstration, we design adhesives with rectangular cut patterns in the shape of the letters, "HELLO" (Supplementary Fig. 15). Lower adhesion can also be achieved by locally reducing width, allowing for adhesive force contrast ratios of over 320x (Supplementary Fig. 16). With selectable adhesion at specific locations, we can go further to design spatially anisotropic adhesion, where a specific region can be programmed to have a prescribed adhesive strength in two directions simultaneously. We spatially programmed adhesion in discrete regions and decoupled the directionality by introducing a second set of rectangular cuts into each adhesive region to independently tune the maximum force in both peel directions (Fig. 4b-e). We can also automate design where the user selects a desired F_{max} in the forward direction ($F_{max,1}$) and backward direction ($F_{max,2}$) for a specific location, then an inverse design algorithm automates a cut pattern and a laser cutter file is generated.

The programmed and experimental adhesion data show strong agreement for three different arbitrary designs, highlighting the ability to reliably create customized, spatially controlled adhesion (Fig. 4f). We next plot the bidirectional enhancement ratios ($F^i_{max,1}/F^{i*}_{max,2}$, where i is the location index) of each region in Fig. 4g. We find good agreement between measured and programmed force ratios for the arbitrarily generated designs and two selected designs to maximize the range of the bidirectional enhancement ratios (See Supplementary Fig. 17). This enables a range of 0.018 - 41, a difference of over three orders of magnitude (\sim 2,300x), showing tremendous ability to program adhesion force in two directions simultaneously at a single region of a film. Chemical and microscale patterns and linear cut features may be able to spatially control adhesion by pinning cracks, but are unable to readily control directional adhesive strength at specific locations as we demonstrate with metamaterial adhesives and our digital fabrication approach.

Demonstrations of metamaterial adhesives

High adhesion yet easy release capabilities are critical for numerous applications. To demonstrate metamaterial adhesives in packaging, we added a layout of cut patterns into a commercial shipping tape, such that strong bonding ensures sealing in all directions yet the adhesive can be removed on demand by peeling in a particular direction (Fig. 5a). A box sealed with metamaterial tape withstood the weight and impact of a brick (1550 g) over 5 drop impacts, while the box sealed with the same tape without metamaterial cuts completely collapsed only after 2 drops (Fig. 5a and b, and Supplementary Video 4). The metamaterial adhesive can also hang objects on a wall, while still being easily removed (Fig. 5c). Furthermore, we used the ability to control adhesion strength in two directions at one location to make the hanging more robust, where adhesion strength was increased at the top and bottom edges to prevent inadvertent release. When hanging a frame with a metamaterial adhesive it remained on a wall over 7 days without any observed delamination and was then easily released (Supplementary Video 5), while the frame supported by an unpatterned adhesive fell off within 20 minutes (Fig. 5d). Metamaterial adhesives can also be applied in wearable form factors. A metamaterial adhesive pick-and-release glove was created by laser-machining non-linear cuts into an elastomer-coated glove. This allowed a user to pick up a flat object, hold it reliably, then effortlessly release the object into a pre-determineded location through wrist rotation, while the unpatterned glove dropped the object (Fig. 5e and f, and Supplementary Video 6).

A metamaterial adhesive strip was also created for a human-in-the-loop wearable device (Fig. 5h). Here the metamaterial adhesive had high adhesion at the edges for strong attachment with easy removal after initial peeling, which was qualitatively observed through significant skin deformation in the F_{max} direction, relative to the unpatterned and F_{min} direction (Fig. 5g). The wearable device, which captures human motion and wirelessly transmits the signal to a mirrored robotic arm, was attached to the arm of a first user where an object was picked, displaced, and released from the robotic arm (Fig. 5i and Supplementary Video 7), and then transferred to another user to move the object again (Fig. 5j and 5k). Cut patterns can also be extended to a variety of adhesive patch shapes, including a circular adhesive patch for a wearable physiological monitoring device (Supplementary Fig. 18).

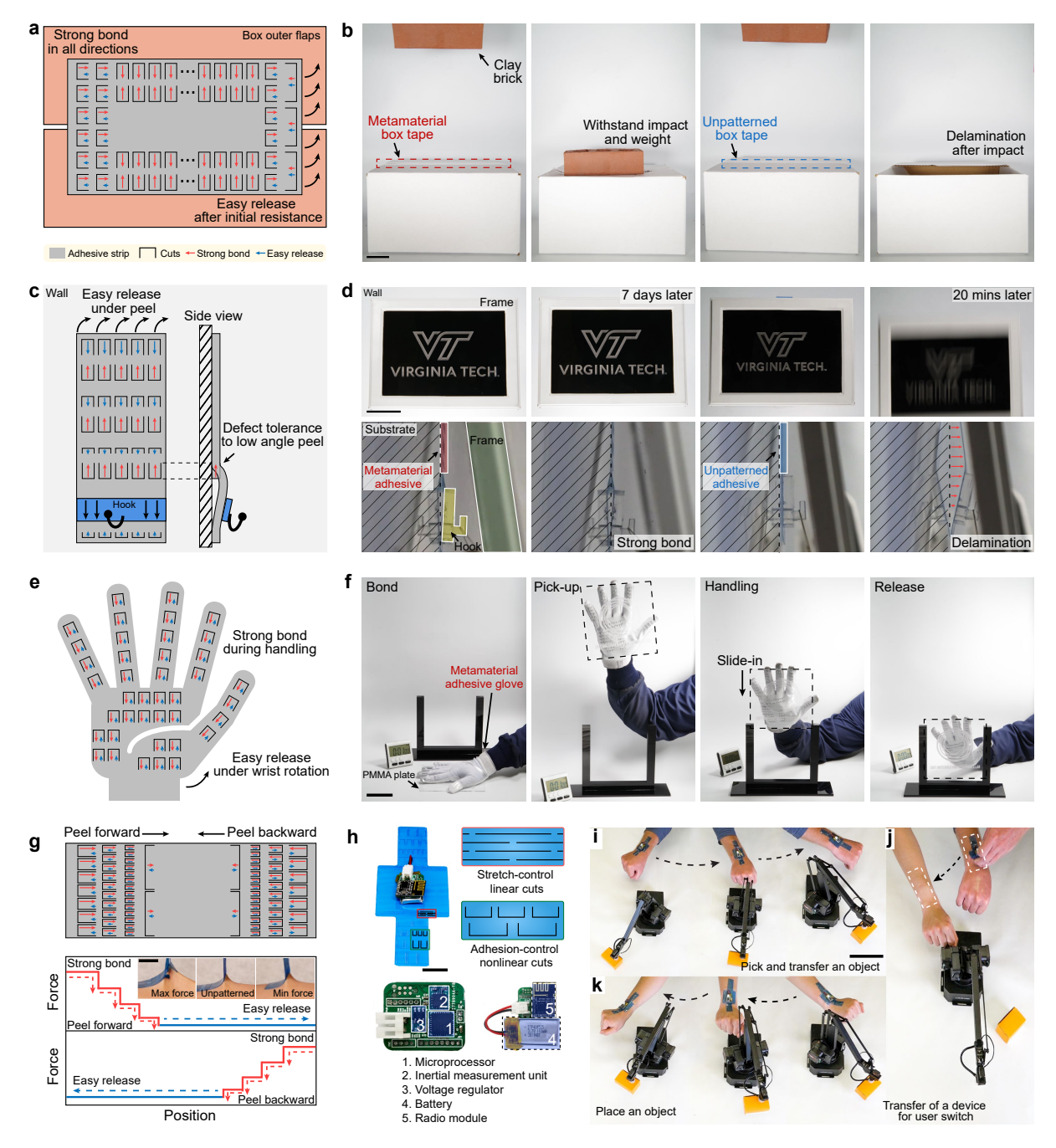


Fig. 5. Metamaterial adhesives with programmable strength and direction. **a**, Metamaterial adhesive box tape design. **b**, A metamaterial adhesive made of box tape holds a box closed during impact of a brick, while a pristine box tape delaminates and fails. Scale bar = 50 mm. **c**, Metamaterial adhesive wall hanging design. **d**, A metamaterial adhesive supports a frame for over 7 days and is then easily removed, while a pristine adhesive fails after 20 minutes. Scale bar = 50 mm. **e**, Metamaterial adhesive glove design. **f**, A metamaterial adhesive glove can pick up flat, fragile objects, transport to a desired area, and then release the object easily. Scale bar = 100 mm. **g**, Metamaterial adhesive wearable patch design. Scale bar = 15 mm. **h**, A wireless wearable motion control device. Scale bar = 15 mm. **i**, An object is picked and transported by a robotic arm controlled by the device adhered to a user's arm. Scale bar = 100 mm. **j**, The device is transferred to another user's arm. **k**, The object is transported and released.

Discussion

Our metamaterial adhesive strategy functions with a range of adhesives on diverse substrates and conditions to enhance adhesion, provide directionality, and spatially program adhesive strength across an adhesive sheet in multiple directions simultaneously. Through a maskless, digital fabrication environment, we can rapidly output diverse adhesive characteristics that cannot be done with chemical or microfeature patterns. Additionally, mm-cm scale cuts could be created with roll-to-roll techniques such as rotary die cutting, providing avenues for scale-up. While our metamaterial adhesive approach works in diverse materials, the cuts introduce locations for possible rupture, and backings that are meant to tear could exacerbate this effect. However, the cut features may also improve tearability, which might be useful for counterfeit protection and easy dispensing of tapes. Our reverse crack propagation mechanism for programmable adhesion may also enable new opportunities in other fracture processes, such as toughening bulk materials, adhesion control in micro/nano systems (See Supplementary Fig. 19 for dimensional scaling predictions), and adhesion for locomotion in robotics. Thus, these metamaterial adhesives can serve as the foundation for the exceptional control of adhesion in diverse materials and applications.

Acknowledgments

D.H., C.L., and M.D.B. acknowledge support from Defense Advanced Research Projects Agency Young Faculty Award (DARPA YFA) (D18AP00041, M.D.B.) and the National Science Foundation under the DMREF program (award number: 2119105, M.D.B.). J.F., B.L., and E.J.M. acknowledge support from the Nebraska Tobacco Settlement Biomedical Research Development funds (E.J.M.). X.Y. and R.L. acknowledge support from the National Science Foundation under the DMREF program (award number: 2118878, R.L.).

Author contributions statement

D.H. and M.D.B. conceived the idea. D.H., C.L., and J.M.G. prepared adhesives and performed experiments. J.F., B.L., and E.J.M. prepared and performed robotic arm and pulse oximetry exper-

iments. D.H., C.L., X.Y. R.L., and M.D.B. analyzed the results. D.H. and M.D.B. wrote the paper with input from E.J.M. and R.L., and M.D.B supervised the study.

Competing interests statement

M.D.B. and D.H. are inventors on a patent application (US Patent 17/248,351) on the adhesive design. The remaining authors declare no competing interests.

References

- 1. A. J. Kinloch, *Adhesion and adhesives: science and technology*. Springer Science & Business Media, 2012.
- N. J. Glassmaker, A. Jagota, C.-Y. Hui, W. L. Noderer, and M. K. Chaudhury, "Biologically inspired crack trapping for enhanced adhesion.," *Proc. Natl. Acad. Sci.*, vol. 104, no. 26, pp. 10786–10791, 2007.
- 3. A. Majumder, A. Ghatak, and A. Sharma, "Microfluidic adhesion induced by subsurface microstructures," *Science*, vol. 318, no. 5848, pp. 258–261, 2007.
- 4. C. Creton and M. Ciccotti, "Fracture and adhesion of soft materials: A review," *Reports Prog. Phys.*, vol. 79, no. 4, p. 046601, 2016.
- I. Hwang, H. N. Kim, M. Seong, S.-H. Lee, M. Kang, H. Yi, W. G. Bae, M. K. Kwak, and H. E. Jeong, "Multifunctional smart skin adhesive patches for advanced health care," *Adv. Healthc. Mater.*, vol. 7, no. 15, p. 1800275, 2018.
- 6. M. D. Dickey, "Stretchable and soft electronics using liquid metals," *Adv. Mater.*, vol. 29, no. 27, p. 1606425, 2017.
- 7. D. E. Packham, "Adhesive technology and sustainability," *Int. J. Adhes. Adhes.*, vol. 29, no. 3, pp. 248–252, 2009.
- 8. B. Chu, K. Jung, C. S. Han, and D. Hong, "A survey of climbing robots: locomotion and adhesion," *Int. J. Precis. Eng. Manuf.*, vol. 11, no. 4, pp. 633–647, 2010.
- S. Kim, J. Wu, A. Carlson, S. H. Jin, A. Kovalsky, P. Glass, Z. Liu, N. Ahmed, S. L. Elgan, W. Chen, P. M. Ferreira, M. Sitti, Y. Huang, and J. A. Rogers, "Microstructured elastomeric surfaces with reversible adhesion and examples of their use in deterministic assembly by transfer printing," *Proc. Natl. Acad. Sci.*, vol. 107, no. 40, pp. 17095–17100, 2010.

- M. A. Graule, P. Chirarattananon, S. B. Fuller, N. T. Jafferis, K. Y. Ma, M. Spenko, R. Kornbluh, and R. J. Wood, "Perching and takeoff of a robotic insect on overhangs using switchable electrostatic adhesion," *Science*, vol. 352, no. 6288, pp. 978–982, 2016.
- 11. H. Lee, B. P. Lee, and P. B. Messersmith, "A reversible wet/dry adhesive inspired by mussels and geckos," *Nature*, vol. 448, no. 7151, pp. 338–341, 2007.
- 12. S. Xia, L. Ponson, G. Ravichandran, and K. Bhattacharya, "Adhesion of heterogeneous thin films ii: Adhesive heterogeneity," *J. Mech. Phys. Solids*, vol. 83, pp. 88–103, 2015.
- 13. H. Yuk, C. E. Varela, C. S. Nabzdyk, X. Mao, R. F. Padera, E. T. Roche, and X. Zhao, "Dry double-sided tape for adhesion of wet tissues and devices," *Nature*, vol. 575, no. 7781, pp. 169–174, 2019.
- 14. J. Yang, R. Bai, B. Chen, and Z. Suo, "Hydrogel adhesion: A supramolecular synergy of chemistry, topology, and mechanics," *Adv. Func. Mater.*, vol. 30, no. 2, p. 1901693, 2020.
- 15. L. Qu, L. Dai, M. Stone, Z. Xia, and Z. L. Wang, "Carbon nanotube arrays with strong shear binding-on and easy normal lifting-off," *Science*, vol. 322, pp. 238–242, 2008.
- 16. L. F. Boesel, C. Greiner, E. Arzt, and A. Del Campo, "Gecko-inspired surfaces: a path to strong and reversible dry adhesives," *Adv. Mater.*, vol. 22, no. 19, pp. 2125–2137, 2010.
- 17. E. P. Chan, E. J. Smith, R. C. Hayward, and A. J. Crosby, "Surface wrinkles for smart adhesion," *Adv. Mater.*, vol. 20, no. 4, pp. 711–716, 2008.
- 18. S. Baik, D. W. Kim, Y. Park, T.-J. Lee, S. Ho Bhang, and C. Pang, "A wet-tolerant adhesive patch inspired by protuberances in suction cups of octopi," *Nature*, vol. 546, no. 7658, pp. 396–400, 2017.
- D.-M. Drotlef, M. Amjadi, M. Yunusa, and M. Sitti, "Bioinspired composite microfibers for skin adhesion and signal amplification of wearable sensors," *Adv. Mater.*, vol. 29, no. 28, p. 1701353, 2017.

- J. Yu, S. Chary, S. Das, J. Tamelier, N. S. Pesika, K. L. Turner, and J. N. Israelachvili, "Geckoinspired dry adhesive for robotic applications," *Adv. Func. Mater.*, vol. 21, no. 16, pp. 3010– 3018, 2011.
- 21. M. K. Kwak, H. E. Jeong, and K. Y. Suh, "Rational design and enhanced biocompatibility of a dry adhesive medical skin patch," *Adv. Mater.*, vol. 23, no. 34, pp. 3949–3953, 2011.
- 22. K. Kendall, "Control of cracks by interfaces in composites," *Proc. R. Soc. A*, vol. 341, no. 1627, pp. 409–428, 1975.
- 23. S. Xia, L. Ponson, G. Ravichandran, and K. Bhattacharya, "Toughening and asymmetry in peeling of heterogeneous adhesives," *Phys. Rev. Lett.*, vol. 108, no. 19, p. 196101, 2012.
- 24. S. Xia, L. Ponson, G. Ravichandran, and K. Bhattacharya, "Adhesion of heterogeneous thin films—i: elastic heterogeneity," *J. Mech. Phys. Solids*, vol. 61, no. 3, pp. 838–851, 2013.
- 25. A. Ghareeb and A. Elbanna, "Extreme enhancement of interfacial adhesion by bulk patterning of sacrificial cuts," *Extreme Mech. Lett.*, vol. 28, pp. 22–30, 2019.
- 26. A. B. Croll, N. Hosseini, and M. D. Bartlett, "Switchable adhesives for multifunctional interfaces," *Adv. Mater. Technol.*, vol. 1900193, pp. 1–20, 2019.
- 27. C. B. Haverkamp, D. Hwang, C. Lee, and M. D. Bartlett, "Deterministic control of adhesive crack propagation through jamming based switchable adhesives," *Soft Matter*, vol. 17, no. 7, pp. 1731–1737, 2021.
- 28. A. Akulichev, A. Tiwari, L. Dorogin, A. Echtermeyer, and B. Persson, "Rubber adhesion below the glass transition temperature: Role of frozen-in elastic deformation," *EPL (Europhysics Letters)*, vol. 120, no. 3, p. 36002, 2018.
- 29. H. Cho, G. Wu, J. Christopher Jolly, N. Fortoul, Z. He, Y. Gao, A. Jagota, and S. Yang, "Intrinsically reversible superglues via shape adaptation inspired by snail epiphragm," *Proc. Natl. Acad. Sci.*, vol. 116, no. 28, pp. 13774–13779, 2019.

- 30. J. Y. Chung and M. K. Chaudhury, "Roles of discontinuities in bio-inspired adhesive pads.," *J. R. Soc. Interface*, vol. 2, no. 2, pp. 55–61, 2005.
- 31. A. Ghatak, L. Mahadevan, J. Y. Chung, M. K. Chaudhury, and V. Shenoy, "Peeling from a biomimetically patterned thin elastic film," *Proc. R. Soc. Lond. A. Math. Phys. Sci.*, vol. 460, no. 2049, pp. 2725–2735, 2004.
- 32. D. G. Hwang, K. Trent, and M. D. Bartlett, "Kirigami-inspired structures for smart adhesion," *ACS Appl. Mater. Interfaces*, vol. 10, no. 7, pp. 6747–6754, 2018.
- 33. R. Zhao, S. Lin, H. Yuk, and X. Zhao, "Kirigami enhances film adhesion," *Soft Matter*, vol. 14, pp. 2515–2525, 2018.
- 34. H. Wang, C. Pan, H. Zhao, T. Wang, and Y. Han, "Design of a metamaterial film with excellent conformability and adhesion for bandage substrates," *J. Mech. Behav. Biomed. Mater.*, p. 104799, 2021.
- 35. H. E. Jeong, J.-K. Lee, H. N. Kim, S. H. Moon, and K. Y. Suh, "A nontransferring dry adhesive with hierarchical polymer nanohairs," *Proc. Natl. Acad. Sci.*, vol. 106, no. 14, pp. 5639–5644, 2009.
- 36. J. T. B. Overvelde, J. C. Weaver, C. Hoberman, and K. Bertoldi, "Rational design of reconfigurable prismatic architected materials," *Nature*, vol. 541, no. 7637, pp. 347–352, 2017.
- 37. D. P. Holmes, "Elasticity and Stability of Shape Changing Structures," *Curr. Opin. Colloid Interface Sci.*, vol. 40, pp. 118–137, 2019.
- 38. T. Chen, M. Pauly, and P. M. Reis, "A reprogrammable mechanical metamaterial with stable memory," *Nature*, vol. 589, no. 7842, pp. 386–390, 2021.
- 39. K. Kendall, "Thin-film peeling-the elastic term," *J. Phys. D. Appl. Phys.*, vol. 8, pp. 1449–1452, 1975.

- 40. J. Steck, J. Kim, J. Yang, S. Hassan, and Z. Suo, "Topological adhesion. i. rapid and strong topohesives," *Extreme Mech. Lett.*, vol. 39, p. 100803, 2020.
- 41. X. Liu, Q. Zhang, Z. Gao, R. Hou, and G. Gao, "Bioinspired adhesive hydrogel driven by adenine and thymine," *ACS Appl. Mater. Interfaces*, vol. 9, no. 20, pp. 17645–17652, 2017.
- 42. J. Li, A. Celiz, J. Yang, Q. Yang, I. Wamala, W. Whyte, B. Seo, N. Vasilyev, J. Vlassak, Z. Suo, *et al.*, "Tough adhesives for diverse wet surfaces," *Science*, vol. 357, no. 6349, pp. 378–381, 2017.
- 43. X. Liu, Q. Zhang, and G. Gao, "Bioinspired adhesive hydrogels tackified by nucleobases," *Adv. Func. Mater.*, vol. 27, no. 44, p. 1703132, 2017.
- 44. H. Yuk, T. Zhang, S. Lin, G. A. Parada, and X. Zhao, "Tough bonding of hydrogels to diverse non-porous surfaces," *Nat. Mater.*, vol. 15, no. 2, pp. 190–196, 2016.
- 45. E. P. Chan, D. Ahn, and A. J. Crosby, "Adhesion of patterned reactive interfaces," *J. Adhes.*, vol. 83, no. 5, pp. 473–489, 2007.
- 46. D. A. Ramrus and J. C. Berg, "Enhancement of adhesion to heterogeneously patterned substrates," *Colloids Surf. A: Physicochem. Eng. Asp.*, vol. 273, no. 1-3, pp. 84–89, 2006.
- 47. A. Ghareeb and A. Elbanna, "Adhesion asymmetry in peeling of thin films with homogeneous material properties: A geometry-inspired design paradigm," *J. Appl. Mech.*, vol. 86, no. 7, 2019.
- 48. D. Sameoto, H. Sharif, J. P. Díaz Téllez, B. Ferguson, and C. Menon, "Nonangled anisotropic elastomeric dry adhesives with tailorable normal adhesion strength and high directionality," *J. Adhes. Sci. Technol.*, vol. 28, no. 3-4, pp. 354–366, 2014.
- 49. M. K. Kwak, H. E. Jeong, W. G. Bae, H.-S. Jung, and K. Y. Suh, "Anisotropic adhesion properties of triangular-tip-shaped micropillars," *Small*, vol. 7, no. 16, pp. 2296–2300, 2011.

50. T.-i. Kim, H. E. Jeong, K. Y. Suh, and H. H. Lee, "Stooped nanohairs: geometry-controllable, unidirectional, reversible, and robust gecko-like dry adhesive," *Adv. Mater.*, vol. 21, no. 22, pp. 2276–2281, 2009.

Methods

Materials

Adhesives films were made with silicone adhesives (Sylgard 184, MG-7 1010 and 9900 Soft Skin Adhesive; Dow Corning), or polyurethane adhesives (VytaflexTM 30; Smooth-On) and backing layers (PET; Grainger and CoTranTM pigmented polyethylene monolayer backing film 9718; 3M, $t = 91 \,\mu\text{m}$). We used commercial Post-it® Note (3M) and MicroporeTM medical surgical tapes (3M) for adhesive fabrication with cut patterns. For adhesion tests that compare commercial adhesives with metamaterial adhesives, we used commercial Post-it® Note (3M), MicroporeTM medical surgical tapes (3M), 101+ making tape (3M), Scotch® MagicTM Greener tape (3M), Scotch® heavy duty shipping packaging tape (3M), and Scotch® multi purpose waterproof duct tape 3960-RD (3M). The G_c values for all commercial adhesives were measured using the same conditions as metamaterial adhesives, using a 90° peel setup at 1 mm/s. For adhesion tests on multiple substrates, we used cast PMMA sheet, borosilicate glass sheet, multipurpose 304 stainless steel bar, multipurpose 6061 aluminum bar and TeflonTM PTFE bar (McMaster-Carr). For coloring samples, we used Silc-PigTM pigments and IgniteTM fluorescent pigments (Smooth-On).

Adhesive preparation

Adhesives were composed of a PET backing layer and a PDMS adhesive layer. A thin PDMS elastomeric layer (20:1 base resin-to-crosslinker ratio; $E = 880 \pm 40$ kPa, $t_{PDMS} \approx 120 \,\mu\text{m}$ or 30:1 base resin-to-crosslinker ratio; $E = 86 \pm 9$ kPa, $t_{PDMS} \approx 120 \,\mu\text{m}$) was created on a glass plate using a thin film applicator (ZUA 2000; Zehntner Testing Instruments) and cured at 80°C for 60 min. PET films ($E = 2.6 \pm 0.1$ GPa) were treated with oxygen plasma (3 min, 300 mTorr oxygen, 400 W, PE-75 Series, Plasma Etch, Inc.), and another layer of PDMS with the same mixing ratio was cast onto the cured PDMS layer using a thin film applicator ($t_{PDMS} \approx 30 \,\mu\text{m}$). The surface treated PET films were placed on the uncured PDMS layer, and the adhesive composite was cured in the oven at 80°C for 60 min. For 20:1 PDMS adhesives, $t_{PET} = 75 \,\mu\text{m}$. For 30:1 PDMS adhesives, $t_{PET} = 125 \,\mu\text{m}$ for Fig. 1f and $t_{PET} = 75 \,\mu\text{m}$ for Fig. 3b. The adhesive composite was then patterned

using a laser machine (Epilog Laser Fusion M2, 75 watt). VHB adhesives were composed of a PET backing layer and a VHB adhesive layer. PET films were treated with oxygen plasma (3 min, 300 mTorr oxygen, 400 W, PE-75 Series, Plasma Etch, Inc.). A VHB layer (75 μ m or 125 μ m) was applied onto the surface treated PET films using a seam roller (Seam Rollers; Marshalltown). For the demonstration of a hanging frame, the adhesives were fabricated with polyurethane elastomers.

Adhesion tests

A 90° peel test setup was utilized to measure the adhesion strength between an adhesive strip and an acrylic substrate on an Instron 5944 mechanical tester with Bluehill 3 software at a constant displacement rate of 1 mm/s. Prior to each run, the adhesive surface of each PDMS specimen was cleaned with isopropyl alcohol. For each specific condition, the same sample was measured repeatedly, except for the commercial adhesives in Figure 1, where distinct samples were measured. The adhesive strip was placed on an acrylic substrate and applied with a rubber roller with a dwell time of 3 min before executing a test. For the underwater test, the adhesive was first immersed in the water for 5 min before being attached to each substrate, and was tested with a dwell time of 3 min. Data obtained from all adhesive tests were analyzed in MATLAB (R2020a). The critical energy release rate G_c of an adhesive strip was calculated by averaging the steady-state adhesion data points obtained from an unpatterned adhesive strip. For the crack analysis, we recorded video during the peel test and the video was analyzed with a video analysis tool (Tracker; Open Source Physics, V5.1.5).

Adhesion simulations

Finite Element Analysis (FEA) for the peeling mechanics of metamaterial adhesives was conducted using ABAQUS software (version 2020). Further details in Supplementary Note 2.

Fabrication of the human robot interface and biomonitoring patch

A silicone adhesive (MG-7 1010 Soft Skin Adhesive; Dow Corning) and a PET layer ($t_{PET} = 50$ μ m) were used to create adhesive patches by following the same fabrication procedures above.

For both demonstrations, the wearable electronics were integrated with the metamaterial adhesive using a silicone adhesive (Sil-poxy; Smooth-On). For the human motion control sensor, the electronics were composed of a microcontroller (STM32; STMicroelectronics), inertia measurement unit (ICM-20948; InvenSense TDK), RF transceiver (nRF24L01+; Nordic), and rechargeable battery with power regulation. The pose of the human arm was estimated by integrating the signal from the three-axis gyroscope. The rotation signal was recorded using an on-board microcontroller, then wirelessly transmitted to another microcontroller that was used to control the robotic arm (uArm Swift Pro; UFACTORY). Once the robotic arm reached the vicinity of a desired location, a preprogrammed sequence of commands was executed to pick, displace, and release an object at a different location. The wearable pulse oximeter (MAX30101, Maxim) was wired to a microcontroller (STM32; STMicroelectronics) using a flexible printed circuit board for signal processing and recording. The recorded signals were normalized and filtered using a low pass filter.

Data availability

All the data and relevant information are available within the article and Supplementary Information. Source data are provided with this paper.